Xian-sheng Wang, Yu-duo Zhang, Qiao-chu Wang, Bo Dong, Yan-jia Wang and Wei Feng*

Photocatalytic activity of Cu_2O/ZnO nanocomposite for the decomposition of methyl orange under visible light irradiation

https://doi.org/10.1515/secm-2018-0170
Received May 23, 2018; accepted July 22, 2018; previously published online November 12, 2018

Abstract: ZnO is modified by Cu_2O by the process of precipitation and calcination. X-ray diffraction has shown that Cu_2O/ZnO catalysts are made of highly purified cubic Cu_2O and hexagonal ZnO. Scanning electron microscopy and transmission electron microscopy have shown that ZnO adhered to the surface of Cu_2O. Due to the doping of Cu_2O, the absorption range of the Cu_2O/ZnO catalyst is shifted from the ultraviolet to the visible region due to diffuse reflection. X-ray photoelectron spectroscopy and photoluminescence spectra have confirmed that there is a substantial interaction between the two phases of the resultant catalyst. The degradation efficiency of Cu_2O/ZnO on methyl orange solution is obviously enhanced compared to Cu_2O and ZnO. The maximum degradation efficiency is 98%. The degradation efficiency is affected by the pH of the solution and initial concentration. After three rounds of recycling, the degradation rate is almost same. This shows a consistent performance of Cu_2O/ZnO. The increase in catalytic ability is related to the lattice interaction caused by the doping of Cu_2O.

Keywords: Cu_2O/ZnO; lattice interaction; methyl orange; visible photocatalysis.

1 Introduction

In recent years, the semiconductor-based photocatalytic technique has been widely used [1] as a promising and effective approach to solve global energy and organic pollutant problems. There are many kinds of the usual photocatalysts, including TiO_2, ZnO, and WO_3. Most of them can react to ultraviolet (UV) light, although the UV light in nature is only 3%–5% and the visible light is about 43% [2]. Therefore, the development of a visible light catalyst [3, 4] is particularly important [5].

ZnO is a wide-band and direct-gap N-type semiconductor, and its band gap is 3.37 eV. It has high photocatalytic activities and hypotoxicity [6]. Thus, ZnO has a potential for the prospective application in the field of photoelectronic devices. However, ZnO can only react to UV light. Several methods have been explored to achieve the goal that ZnO does respond to visible light, such as ion doping [6], noble metal deposition [7], semiconductor coupling [8], and surface sensitization [9], and coupling with a semiconductor has been useful to achieve high photocatalytic activities of most regions of visible light. At the University of California, Wadia et al. [10–12] studied 23 kinds of inorganic semiconductor potential materials. They found nine promising inorganic semiconductor photovoltaic materials, including FeS, Cu_2S, Zn_3P_2, Cu_2O, CuO, NiS, PbS, α-Si, and CZTS. Semiconductor materials that can be used for coupling include V_3O_4 [13], CuO [14], and Cu_2O [15–17]. Cu_2O is a kind of traditional photoelectronic p-type semiconductor with a band gap of about 2.1 eV. Cu_2O has a high absorption coefficient in the visible light region. Doping of Cu_2O can increase the catalytic ability in visible light, which can decrease the cost in practice. Also, hurt to human caused by UV light can be avoided.

Wu et al. prepared different shapes of Cu_2O/ZnO and studied photocatalytic activity but did not examine the catalytic activity of visible light [16]. Lahmar et al. did grow Cu_2O/ZnO on fluorine-doped tin oxide using the electrodeposition method and tested electrical characteristics [17]. Geioushy et al. fabricated and tested graphene/ZnO/Cu_2O electrodes for CO_2 electroreduction in the $NaHCO_3$ electrolyte [18]. Hong et al. tested Cu_2O/ZnO film using the electrodeposition method. The degradation efficiency for formaldehyde of the composite was 80.33% for visible light irradiation [19].

In this paper, Cu_2O/ZnO is successfully obtained by calcination. Compared to materials prepared by other methods, the composite is stable, low cost, and easy to fabricate. Additionally, it is nontoxic and harmless. Therefore, Cu_2O/ZnO has some advantage in practice. It can make full use of visible light when used to degrade methyl orange

***Corresponding author: Wei Feng,** Key Lab of Groundwater Resources and Environment, Ministry of Education, Jilin University, Changchun 130021, P.R. China, e-mail: weifeng@jlu.edu.cn
Xian-sheng Wang, Yu-duo Zhang, Qiao-chu Wang, Bo Dong and Yan-jia Wang, Key Lab of Groundwater Resources and Environment, Ministry of Education, Jilin University, Changchun 130021, P.R. China

(MO). The microstructure and performance of the composite are studied by X-ray diffraction (XRD), scanning electron microscopy (SEM), transmission electron microscopy (TEM), and diffuse reflection. X-ray photoelectron spectroscopy (XPS) is carried out to explore the mechanism behind the process. The results show that there is the p-n heterostructure in hybrid powder and the composite has excellent photocatalytic performance. The mechanism of Cu_2O/ZnO is in accordance with the mechanism of photoinduced electron transfer.

2 Materials and methods

2.1 Materials

Zinc nitrate pentahydrate [$Zn(NO_3)_2{\cdot}5H_2O$] and MO were bought from Huachang Pharmaceutical Co., Ltd. Anhydrous sodium carbonate (Na_2CO_3), copper acetate monohydrate [$Cu(CH_3COO)_2{\cdot}H_2O$], glucose, sodium hydroxide (NaOH), acetic acid (CH_3COOH), and anhydrous ethanol (C_2H_5OH) were purchased from Beijing Chemical Reagent. All chemical reagents were in AR and used as received.

2.2 Preparation

$Zn(NO_3)_2{\cdot}5H_2O$ (5.95 g) and Na_2CO_3 (14.10 g) were both dissolved in 100 ml deionized water. With magnetic stirring, the Na_2CO_3 solution was added drop by drop to the solution of 100 ml $Zn(NO_3)_2$; a white precipitate is then formed. The mixed solution was washed and filtered with deionized water several times to obtain a white precipitate. The white precipitate was dried in a blast oven at 100°C for 2 h. Then, the dried precipitate was fired at a muffle furnace at 400°C for 2 h; the ZnO nanomaterial was then obtained.

$Cu(AC)_2{\cdot}H_2O$ was dissolved in 50 ml absolute ethanol to obtain different concentration solutions of $Cu(AC)_2$ (0, 0.028, 0.056, 0.084, and 0.112 mol/l), and 0.3 g ZnO was dispersed in the above solution under sonication for 30 min. HAC (2 ml) was added drop by drop to the above solution and the above solution was kept in a constant temperature water bath at 60°C with magnetic stirring. Then, 0.17 mol/l glucose solution (50 ml) was added to the above solution at a rate of 6 ml/min, and 1 mol/l NaOH solution (60 ml), deionized water (25 ml), and absolute ethanol (35 ml) were added drop by drop under the same conditions to the above solution. When a dark yellow precipitate appeared, stirring was continued for 30 min. The precipitate was washed three times with absolute ethanol and deionized water and dried in a vacuum oven at 60°C for 8 h. Cu_2O/ZnO, which was prepared with the ratio of Cu_2O to ZnO of 0.39, 0.78, 1.17 and 1.56, were labeled as samples I–IV, respectively. Pure Cu_2O was prepared without the dispersing ZnO.

2.3 Instrumental analysis

XRD patterns were measured with XRD (D8 Advanced XRD, XD-3, Japan) with CuKα radiation source ($\lambda = 0.15418$ nm). XRD patterns were obtained with diffraction angles 2θ ranging from 20° to 80°. The microstructure of the catalyst was observed by SEM (Philips XL-30, Japan). TEM (ASAP2010M, Norcross, GA, USA) images of the samples were obtained on a FEI-Tecnai F20ST electron microscope by fixing the powder of the catalyst to a 3 mm copper grid. UV-visible (UV-vis) spectrum was obtained on a UV-vis Cintra-10e spectrometer (UV-1700, Japan) with a wavelength range of 200–800 nm. The basic element composition and binding state of the catalyst were studied by XPS (ESCALAB 250, Thermo Fisher Scientific, Waltham, MA, USA). The photoluminescence (PL) analysis was performed on a spectrometer (F-4500, Japan), using a Xe lamp (excitation at 365 nm) as the light source.

2.4 Photocatalytic studies

The effect of the sample was evaluated by degrading MO [13]. At room temperature, 0.100 g of samples I–IV, pure ZnO, and pure Cu_2O were added to 100 ml MO solution of different concentration. The pH was controlled by the addition of HCl. The solution was stirred for 30 min without illumination. After sampling, the solution was kept under a 300 W hernia lamp using JZ-420 filter to filter out the light below 420 nm. The MO solution with the catalyst was irradiated and stirred for 4 h; in the process, samples were taken every 30 min. After centrifugation, the supernatant was collected and analyzed by UV spectrophotometry, and the concentration of MO was calculated by 464 nm absorbance. The photodegradation rate of MO (D) was measured using the following formula for calculation:

$$D = [(C_0 - C)/C_0] \times 100\%$$

where C_0 and C are the MO concentrations at time 0 and t (irradiation time).

3 Results and discussion

Figure 1 shows the XRD patterns of Cu_2O/ZnO with different Cu_2O concentrations. The XRD of pure ZnO and pure Cu_2O is also studied for contrast. According to the

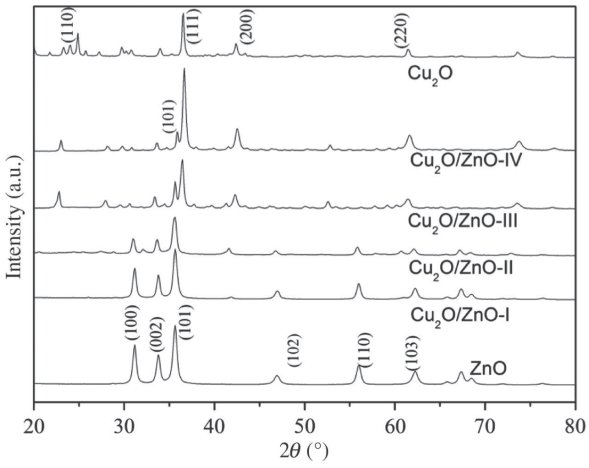

Figure 1: XRD patterns of Cu_2O/ZnO prepared with different Cu_2O concentrations.

diffraction card JCPDS05-0667, the prepared pure Cu_2O is assigned to the cubic phase and the main facets of the cubic phase of Cu_2O (111), (110), (200), and (220) [17, 20] appeared at $2\theta = 36.418°$, 29.554°, 42.297°, and 61.466°, respectively. After doping, there is no distinct change observed in the crystallite size. There is no obvious difference between the diffraction peaks of ZnO and the diffraction peaks of the hexagonal wurtzite (JCPDS89-0511) reported in the literature. The main facets [21] of ZnO (100), (101), (002), (102), and (103) [18, 22, 23] appeared at $2\theta = 31.769°$, 36.525°, 34.421°, 47.538°, and 62.220°, respectively, and there are no obvious peaks of any other phase or impurities [6]. There is little displacement between (103) and (220), which could illustrate the presence of lattice interaction. The lattice interaction means p-n heterojunctions. TEM further demonstrated the statement. Further, the result of XPS indicated the interaction of Cu_2O/ZnO responsible for activation by visible light. As the ratio of Cu_2O to ZnO increased, the diffraction peak of Cu_2O was enhanced obviously, which indicate that the samples of Cu_2O have a good crystal structure. These catalysts are made of highly purified Cu_2O and ZnO, their crystal structures are not destroyed, and there are no new characteristic diffraction peaks.

The SEM images of ZnO (A), Cu_2O (B), and Cu_2O/ZnO (sample II; C) and the energy-dispersive X-ray spectroscopy (EDX) of Cu_2O/ZnO (sample II; D) are shown in Figure 2. It reveals that the prepared ZnO is hexagonal wurtzite nanoparticle with an average particle size of 60 nm. The prepared Cu_2O is a homogeneous spherical nanoparticle with an average particle size of about 500 nm. In Figure 2B and C, it can be found that after combining with ZnO the smooth surface of spherical Cu_2O becomes rough because the Cu_2O surface is covered by a lot of ZnO nanoparticles. The result of EDX shows that no any other secondary phase exits.

Figure 3 shows the mapping of Cu_2O/ZnO. This illustrates that there are O, Zn, and Cu elements on the surface of Cu_2O/ZnO. The O element is basically distributed in the whole SEM image and the Zn element is also scattered in the picture. However, in the position where the sphere is more, the Cu element is more concentrated and the O and Zn elements are sparser compared to other locations. Cu exists in the form of Cu_2O, and ZnO is present on the surface of Cu_2O.

The TEM and high-resolution TEM (HR-TEM) images of Cu_2O/ZnO (sample II) are shown in Figure 4. ZnO nanoparticles adhered to the surface of Cu_2O with a diameter of about 500 nm, which is consistent with the SEM image. In Figure 4B, the close contact of Cu_2O and ZnO could be observed clearly, where the stripes interval at 0.151 nm and 0.148 nm can be attributed to the lattice face value of cubic phase Cu_2O (220) and hexagonal wurtzite (103). Figure 4B obviously shows the existence of an interaction between Cu_2O/ZnO nanoparticles. The TEM result further confirms the XRD result.

Figure 5A–C shows the Cu_{2p}, Zn_{2p}, and O_{1s} XPS spectra of Cu_2O, ZnO, and Cu_2O/ZnO (sample II), respectively. In Figure 5A, the peaks of pure Cu_2O at 932.4 and 952.0 eV are related to the binding energy of $Cu_{2P3/2}$ and $Cu_{2P1/2}$, which is consistent with the Cu^+ species [18, 24–26]. Compared to the peaks of pure Cu_2O, the binding energy of Cu_2O/ZnO peaks shift at 0.1 eV to lower binding energy. In Figure 5B, the characteristic peaks of pure ZnO at 1022.2 and 1045.4 eV are mainly consisted of $Zn_{2P3/2}$ and $Zn_{2P1/2}$ in ZnO [27]. In Figure 5, the binding energies of $Zn_{2P3/2}$ and $Zn_{2P1/2}$ in Cu_2O/ZnO are obviously higher than that in pure ZnO. Figure 5C shows the O_{1s} XPS spectra of pure ZnO, Cu_2O/ZnO, and pure Cu_2O. The characteristic peak of Cu_2O/ZnO at 529.6 eV corresponds to the lattice of Cu_2O and ZnO. The pure ZnO peak at 527.6 eV corresponds to the oxygen in the lattice of ZnO. The peak of pure Cu_2O at 529.8 eV corresponds to the oxygen in the Cu_2O lattice. The source of the characteristic peak of pure Cu_2O at 531.8 eV, the peak of pure ZnO at 529.4 eV, and the peak of Cu_2O/ZnO at 531.2 eV are more complex and may correspond to oxygen deficiencies and surface-adsorbed oxygen. The binding energy of the oxygen in the Cu_2O/ZnO lattice is higher and lower than the binding energy of the oxygen in the ZnO and Cu_2O lattice, which illustrates that the reaction between lattice O and Zn has become weaker and the one between lattice O and Cu has become stronger. This is obvious evidence of lattice interaction.

The UV-vis spectra of Cu_2O/ZnO prepared with different concentrations of Cu_2O are shown in Figure 6. UV-vis spectra are studied to compare to pure ZnO and

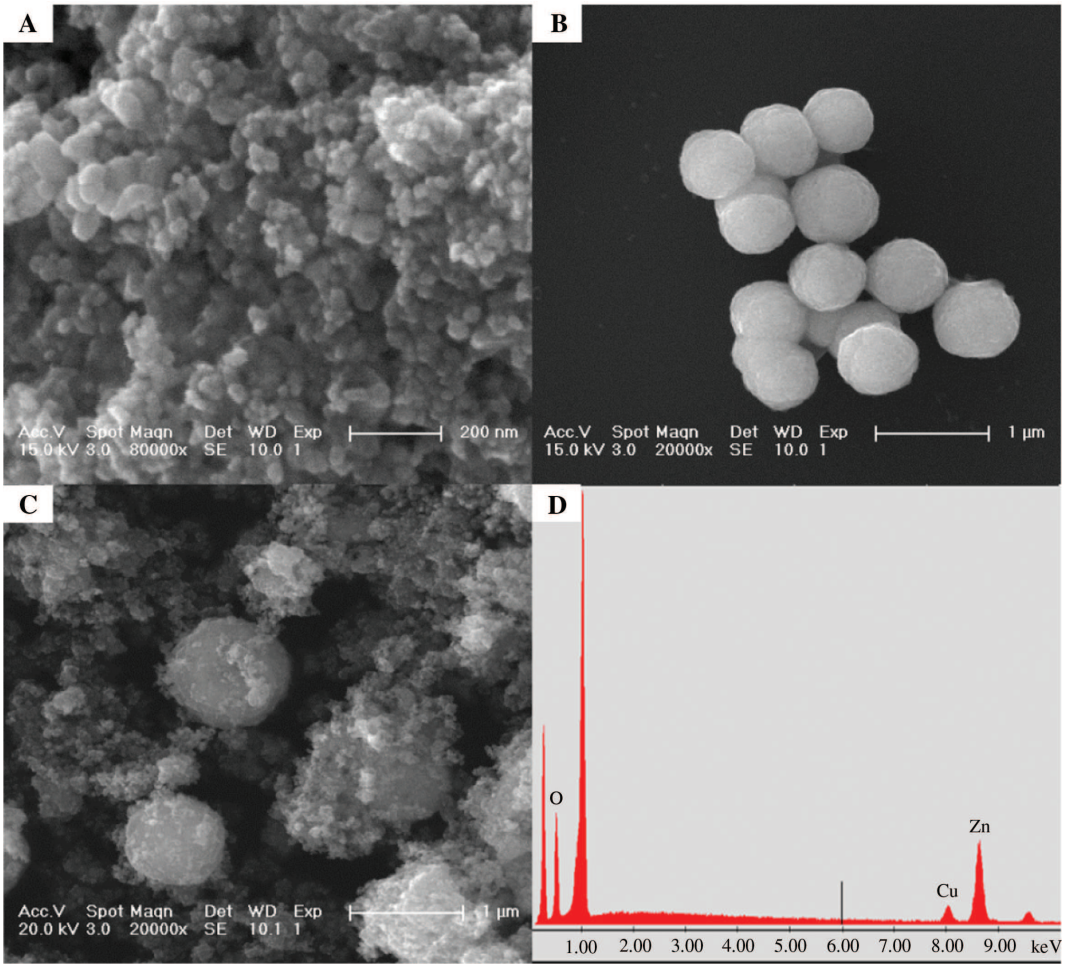

Figure 2: SEM images of ZnO (A), Cu_2O (B), and Cu_2O/ZnO (sample II; C) and EDX of Cu_2O/ZnO (sample II; D).

pure Cu_2O. The results indicate that all the samples have light absorption with different degrees in the range of 200–800 nm. These samples can effectively absorb light, which laid the foundation for the photocatalysis of the catalyst under visible light. From the curve, the initial absorption edge of pure ZnO samples is at 380 nm, the initial absorption edge of Cu_2O samples is at 590 nm, and the initial absorption edge of Cu_2O/ZnO I–IV is at 680, 600, 630, and 620 nm, respectively. After the doping of Cu_2O, the absorption range in the visible light of the Cu_2O/ZnO catalyst is obviously larger than the pure ZnO and the pure Cu_2O. With the increase of Cu_2O content, the absorption range gradually increases and then decreases, which could be explained by the utilization of photons. The lower ratio of Cu_2O to ZnO did not have enough p-n heterojunctions. The higher ratio caused the decrease of the Cu_2O area that is irradiated by visible light, which caused the decrease of the interface area [28] between Cu_2O and photons. Many photons are wasted. The absorption range of sample II is the largest. The absorption energy levels of samples ZnO, Cu_2O, and I–IV are calculated by the following formula:

$$\mathrm{Eg} = \frac{hc}{\lambda}$$

where Eg is the absorption energy level, h is the Plank constant (4.135667×10^{-15} eV s), c is the speed of light (3×10^8 m/s), and λ is the absorption wavelength.

The absorption energy levels of samples ZnO, Cu_2O, and I–IV are 3.26, 2.1, 1.8, 2.1, 1.97, and 2 eV, respectively, and the absorption range of the Cu_2O/ZnO catalyst is shifted from UV region to visible light, which further demonstrates its photocatalytic prospects under visible light.

The relationship between degradation efficiency, time, and doping ratio under visible light is shown in Figure 7A. The corresponding kinetic plots are shown in Figure 7B. In Figure 7, all Cu_2O/ZnO catalysts have better photocatalytic activity than pure ZnO and Cu_2O in visible light irradiation. ZnO has nearly no degradation effect on

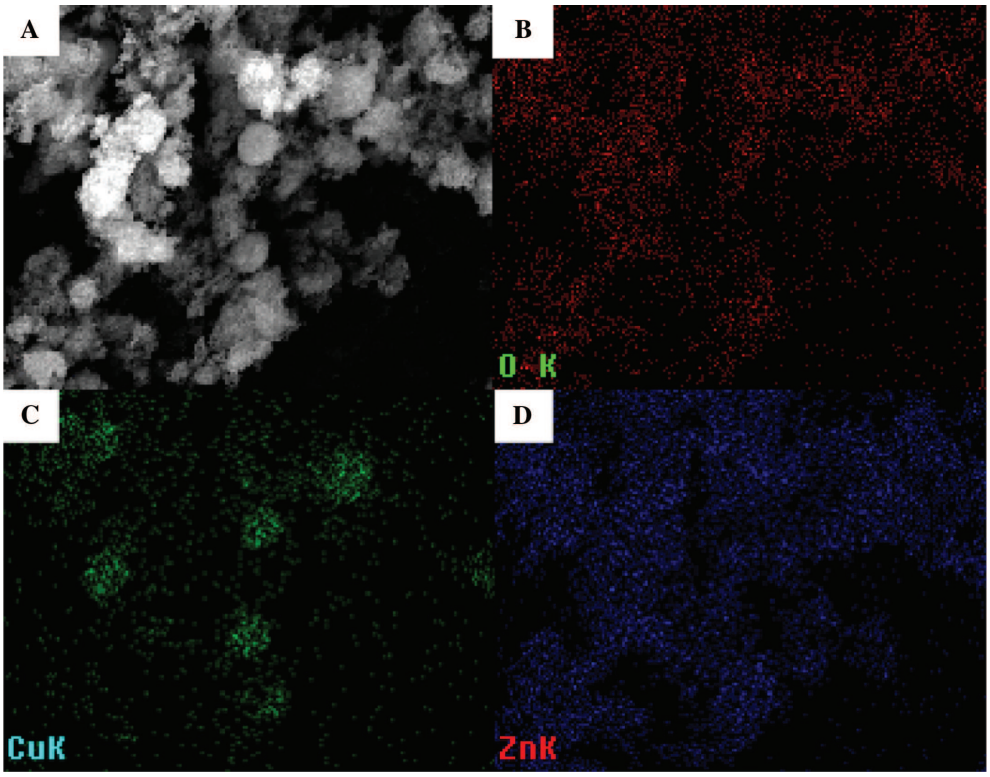

Figure 3: Mapping of Cu_2O/ZnO (sample II). Cu_2O/ZnO (A), distribution of O (B), Cu (C), Zn (D).

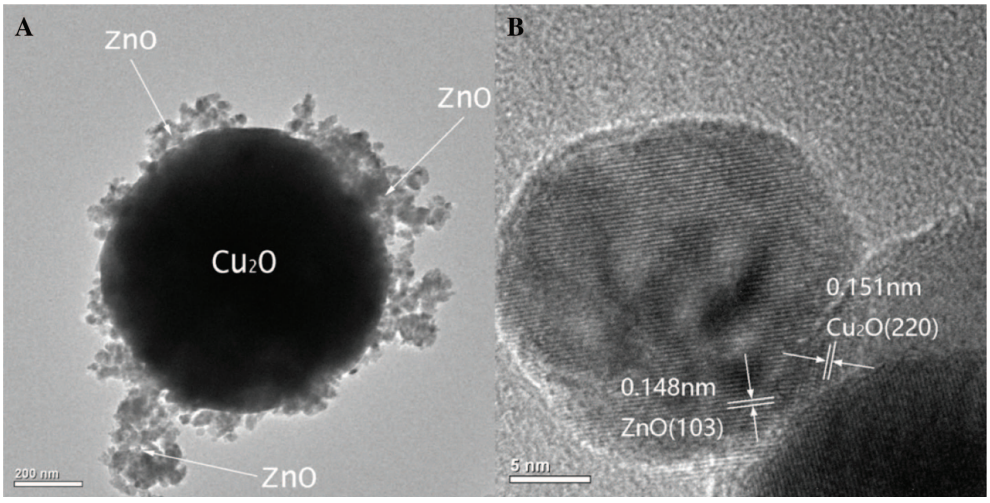

Figure 4: TEM images (A) and HR-TEM images (B) of Cu_2O/ZnO (sample II).

the visible region of $\lambda > 420$ nm. This may be due to the adsorption of ZnO on the MO. On the contrary, the number of defective sites is the most important factor leading to the result, such as oxygen vacancy and interstitial zinc atom, and to the acceptor states that arise from zinc vacancies and interstitial oxygen atoms [29]. The degradation rate of Cu_2O is 30% in 120 min, but it does not have extinct change after 120 min, which may ascribe to the recombination of photoinduced electrons and holes [30]. The best ratio of Cu_2O to ZnO is 0.78, which agrees with the result of UV-vis. This could be explained by the utilization of photons. The lower ratio did not have enough p-n heterojunctions and the higher ratio has caused the decrease of the interface area between Cu_2O and photons. To describe quantitatively, we have used the kinetic model fitting the process of MO degradation. Results show that photocatalysis is first-order reaction kinetics: $k_{II} > k_{III} > k_{IV} > k_I > k_{Cu_2O} > k_{ZnO}$, $k_{II} = 2.75k_{III}$. Thus,

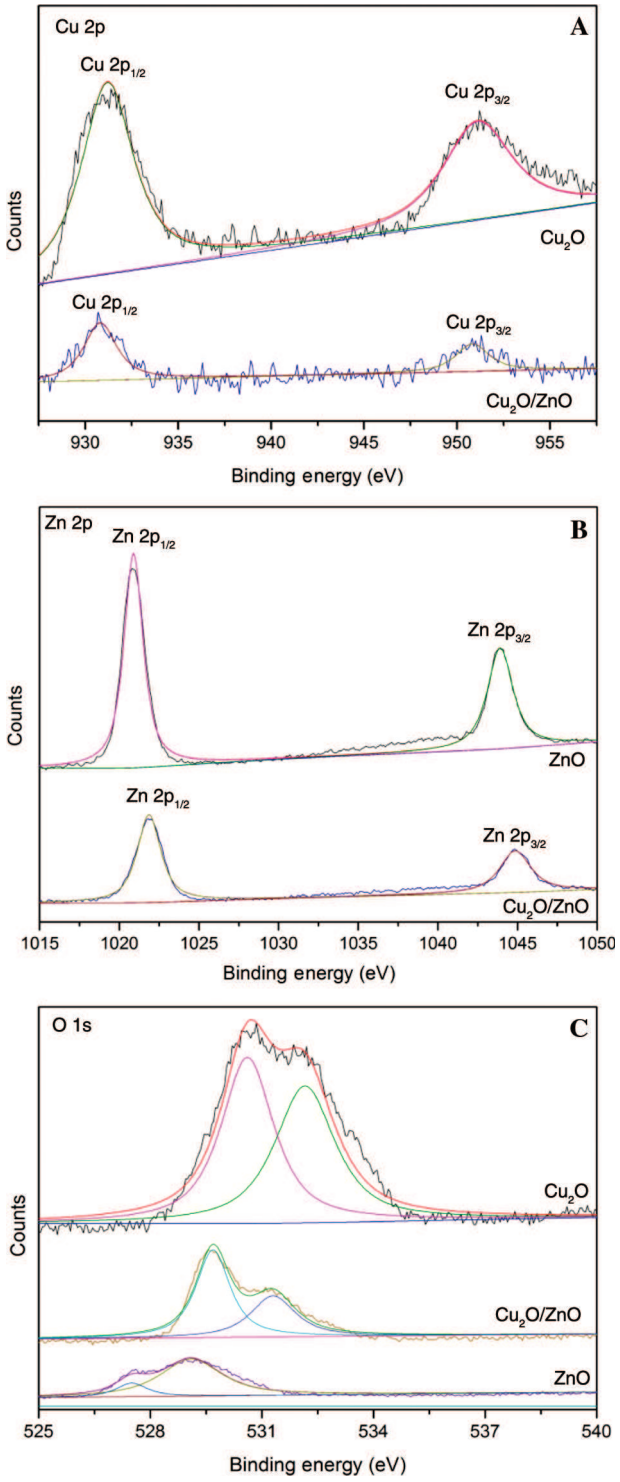

Figure 5: XPS images of Cu_2O/ZnO (sample II), pure Cu_2O, and pure ZnO and Gaussian deconvolution of Cu 2p (A), Zn 2p (B), O 1s (C).

when the Cu_2O concentration is 0.056 mol/l and the MO concentration is 50 mg/l, the photocatalytic degradation of the prepared Cu_2O/ZnO catalyst is the best, and MO has been completely degraded at 180 min.

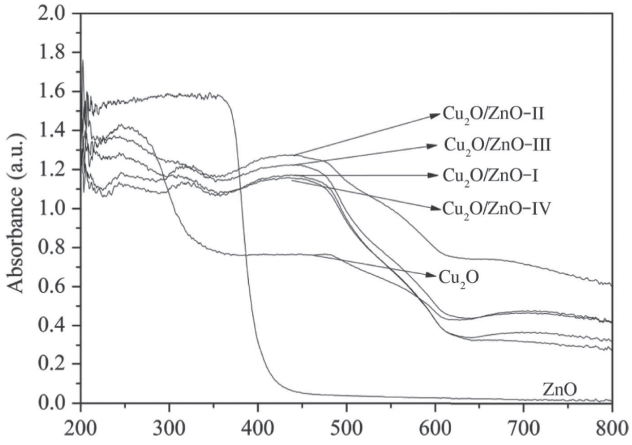

Figure 6: UV-vis spectra of Cu_2O/ZnO prepared with different Cu_2O concentrations.

The UV-vis spectrum of the photodegradation efficiency of MO by Cu_2O/ZnO (sample II) with degradation time is shown in Figure 8. The curve [31] demonstrates that the absorption of MO gradually decreases to 0 as the reaction progresses, which indicates that MO has been completely degraded at 3 h.

Figure 9 shows the degradation efficiency of the initial concentrations of different MO with Cu_2O/ZnO (sample II). The curve reveals that the initial concentration of MO has a great effect on the photodegradation. To describe quantitatively, we have used the kinetic model fitting the process of MO degradation. Results show that $k_{50} > k_{100} > k_{200} > k_{300}$, $k_{50} = 2.79k_{100}$.

Thus, as the initial concentration increases from 50 to 300 mg/l, the rate of photodegradation gradually decreases, because the larger MO concentration causes the heavier solution color; thus, light transmittance is affected. Furthermore, MO and its intermediates have occupied the active sites of the Cu_2O/ZnO catalyst, which decreases the reactivity.

The degradation efficiency of 100 mg/l MO with Cu_2O/ZnO (sample II) in different pH is shown in Figure 10. The pH of the solution has a great effect on the photodegradation efficiency. To describe quantitatively, we have used the kinetic model fitting the process of MO degradation. Results show that $k_{3.8} > k_{4.8} > k_{6.8} > k_{5.8} > k_{2.8}$, $k_{3.8} = 1.89k_{4.8}$, With the higher pH of the solution, the degradation rate sharply increases first and then decreases gradually. When the pH of solution is equal to 3.8, the reaction speed is the highest.

Thus, the photocatalytic degradation of pH (=3.8) is the best when the catalyst is sample II, and the MO concentration is 100 mg/l and the largest degradation efficiency is 98%.

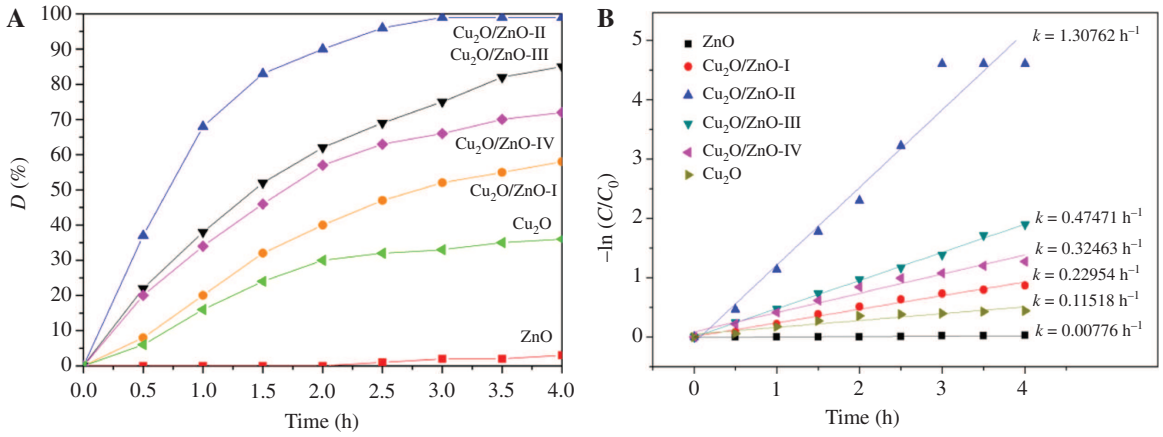

Figure 7: Photocatalytic activity of Cu_2O/ZnO prepared with different Cu_2O concentrations (A) and kinetic plot of MO degraded with Cu_2O/ZnO prepared with different Cu_2O concentrations (B; catalyst 0.1 g; initial concentration of MO 50 mg/l; pH 6.8).

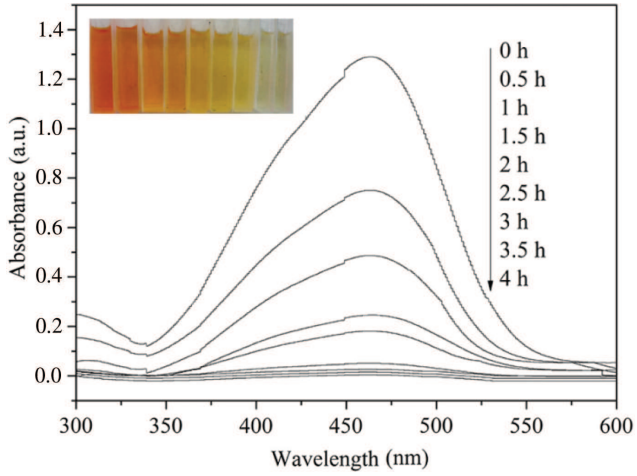

Figure 8: UV-vis spectra of using Cu_2O/ZnO (sample II) photodegrade MO with the degradation time.

Figure 11 is used to study the reproducibility of Cu_2O/ZnO (sample II) in case of degradability. The spent catalyst, after centrifugation and drying, is repeatedly used to treat the solution with 50 mg/l MO. Cu_2O/ZnO has good repeatability as used in degradation.

It is well known that benzoquinone (BQ) and isopropyl alcohol (IPA) can be used to remove $\cdot O^{2-}$ and ·OH, respectively. EDTA is an effective scavenger for photoinduced holes (h^+) [32–34].

In Figure 12, EDTA and IPA have a stronger inhibitory effect on the photodegradation of MO with Cu_2O/ZnO than BQ, which indicates that h^+ and ·OH are the main active groups. To describe quantitatively, we have used the kinetic model fitting the process of MO degradation. Results show that $k_{normal} > k_{BQ} > k_{EDTA} > k_{IPA}$, and BQ, EDTA, and IPA decrease normal degradation rates by 39.98%, 66.73%, and 80.36%, respectively.

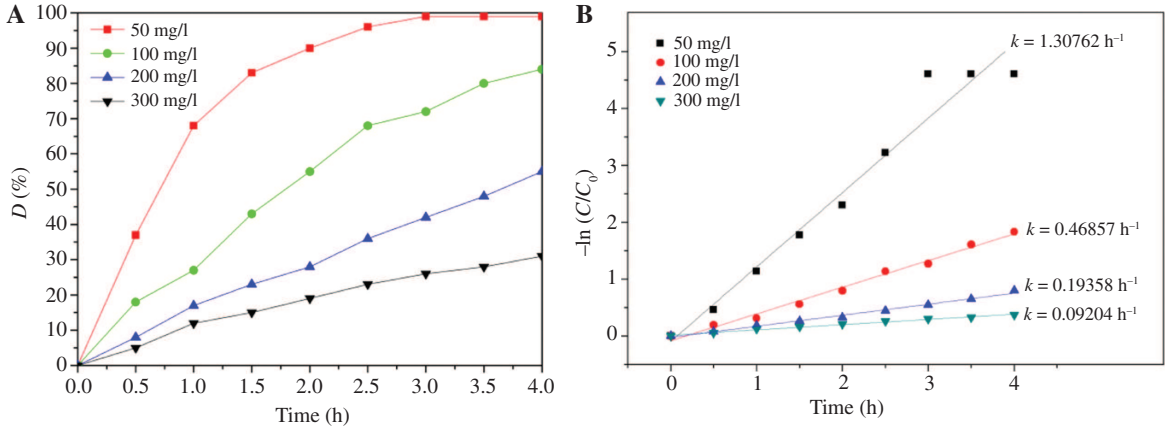

Figure 9: Map (A) and kinetic plot (B) of the degradation of the different initial concentrations of MO with Cu_2O/ZnO (sample II; catalyst 0.1 g; pH 6.8).

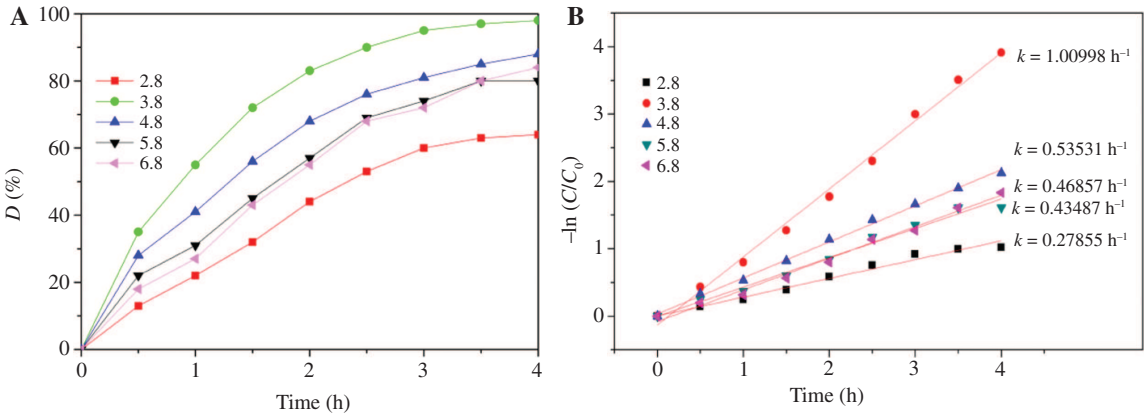

Figure 10: Map (A) and kinetic plot (B) of the degradation of MO with Cu_2O/ZnO (sample II) with different pH (catalyst 0.1 g; initial concentration of MO 100 mg/l).

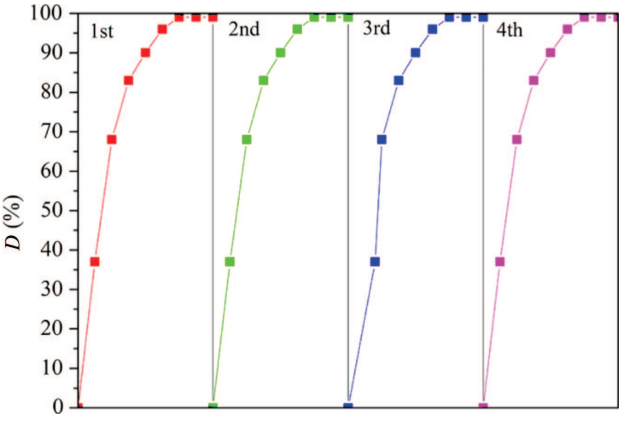

Figure 11: Map of MO degradation used Cu_2O/ZnO (sample II) repeatedly (catalyst 0.1 g; initial concentration of MO 50 mg/l; pH 6.8).

According to the results of this trapping experiment, the possible process of MO photodegradation with the Cu_2O/ZnO catalyst can be proposed by the following equations [35]:

$$Cu_2O/ZnO + h\upsilon \rightarrow Cu_2O/ZnO\,(h^+ + e^-)$$

$$e^- + O_2 \rightarrow \cdot O_2^- + H_2O \rightarrow \cdot OH$$

$$h^+ + H_2O \rightarrow \cdot OH$$

$$\cdot OH/h^+ + MO \rightarrow \text{degradation products}$$

Theoretical analysis shows that the main reason for the enhanced photocatalytic activity of Cu_2O/ZnO can be attributed to the absorption band edge of ZnO and Cu_2O and the heterogeneous structure formed between them. Figure 13 shows the diagram of the absorption band edge of ZnO and Cu_2O and the charge transferred under visible light irradiation. Because of the energy of narrow bandgap, Cu_2O can produce electron-hole pairs in visible light. The conduction band and valence band of Cu_2O are

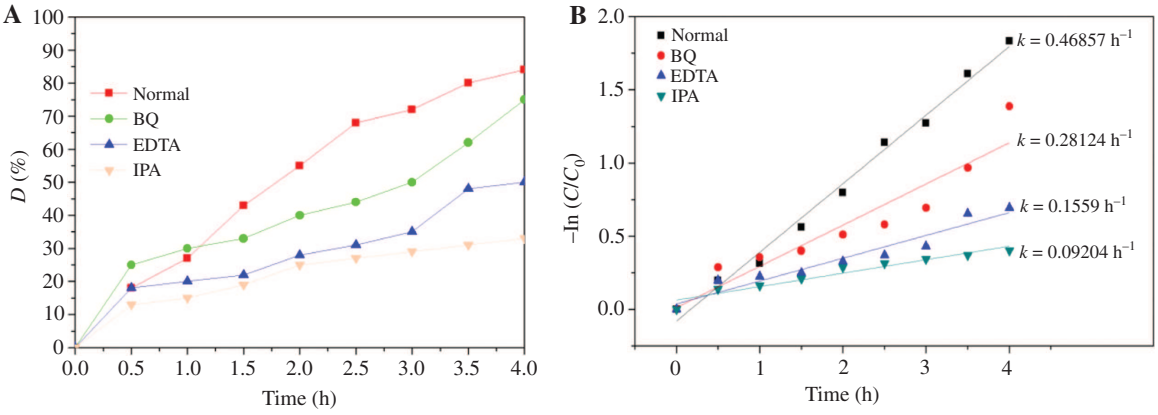

Figure 12: Map (A) and kinetic plot (B) of MO photodegradation with Cu_2O/ZnO with the presentation of BQ, EDTA, and IPA.

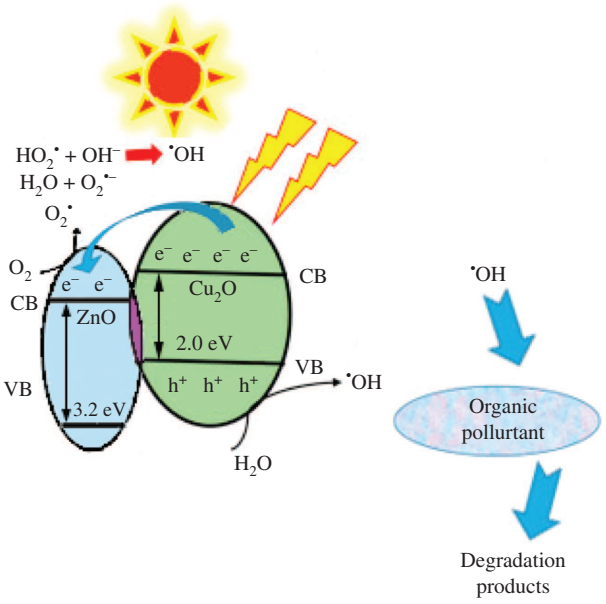

Figure 13: Diagram of the absorption band edge of ZnO and Cu_2O and the charge transfer under visible light irradiation.

−1.6 and +0.4 eV, respectively, and Cu_2O is more negative than ZnO (the conduction band and valence band of ZnO are −0.3 and +2.9 eV, respectively), which result in the generation of electrons from the Cu_2O conduction band transferred to the ZnO conduction band. At the same time, the p-n heterogeneous structure is formed by the contact between the n-type semiconductor ZnO and the p-type semiconductor Cu_2O, which further improves the transmission of the photogenerated electron-hole pairs by the difference of potential energy.

The PL spectra results of pure ZnO and Cu_2O/ZnO (sample II) are shown in Figure 14. With the doping of Cu_2O, the peaks in the range of 350–400 nm shifted to visible range, which demonstrates the decreasing of bandgap. In the range of 400–470 nm, compared to pure ZnO, a weaker peak can be observed in Cu_2O/ZnO (sample II), which indicates that the charge transfer between ZnO and Cu_2O would suppress the recombination of electron-hole pairs [27]. The peaks at about 520 nm can be attributed to vacancy and defect of O and the addition of Cu_2O increased the vacancies and defects. The vacancy and defect also can inhibit the recombination of electron-hole pairs. Thus, the PL spectra are consistent with the previous mechanism.

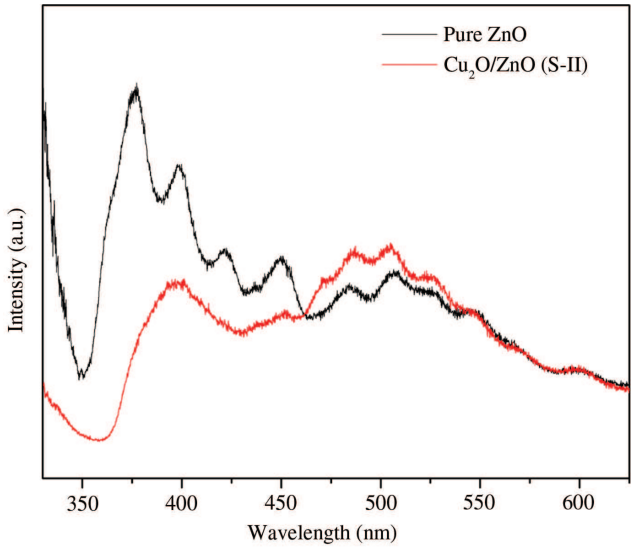

Figure 14: PL spectra of pure ZnO and Cu_2O/ZnO (sample II).

4 Conclusions

Cu_2O/ZnO is prepared by precipitation and calcination. ZnO covers the surface of spherical Cu_2O, and the structures of Cu_2O and ZnO are not deformed during the doping process. There is a strong interaction existing between Cu_2O and ZnO. The visible light photocatalytic ability is obviously enhanced because of the presence of lattice interaction. When the ratio of Cu_2O to ZnO is 0.78, the degradation of MO is the best. The maximum degradation efficiency is 98%, and Cu_2O/ZnO has good repeatability. h^+ and ·OH are the main active groups in the process of degradation. This concludes that the lattice interaction can enhance the photocatalytic ability.

Acknowledgments: This work was supported by the National Natural Science Foundation of China (No. 61774073) and the Science and Technology Development Program of Jilin Province (No. 20170101086JC).

References

[1] Luo J, Zhou X, Ma L, Xu X. *Appl. Surf. Sci.* 2016, 390, 357–367.
[2] Wang X, Sun Y, Liu C, Feng W, Zou D. *Rsc Adv.* 2015, 5, 49153–49158.
[3] Luo J, Zhou X, Ning X, Zhan L, Huang L, Cai Q, Li S, Sun S. *Mater. Res. Bull.* 2018, 100, 102–110.
[4] Luo J, Zhou X, Ning X, Zhan L, Ma L, Xu X, Li S, Sun S. *Separ. Purif. Technol.* 2018, 201, 309–317.
[5] Dai D, Xu H, Ge L, Han C, Gao Y, Li S, Lu Y. *Appl. Catal. B Environ.* 2017, 217, 429–436.
[6] Liu X, Yang Y, Han Y, Wang L, Chen G, Xiao X, Wang Y. *J. Nanostruct.* 2017, 7, 82–87.
[7] Huang Q, Li J. *Mater. Lett.* 2017, 204, 85–88.
[8] Harish S, Archana J, Sabarinathan M, Navaneethan M, Nisha KD, Ponnusamy S, Muthamizhchelvan C, Ikeda H, Aswal DK, Hayakawa Y. *Appl. Surf. Sci.* 2017, 418, 103–112.
[9] Chava RK, Kang M. *Mater. Lett.* 2017, 199, 188–191.
[10] Wadia C, Alivisatos AP, Kammen DK. *Environ. Sci. Technol.* 2009, 43, 2072–2077.

[11] Luo Y, Wang L, Zou Y, Sheng X, Chang L, Yang D. *Electrochem. Solid State Lett.* 2012, 15, H34–H36.
[12] Herion J, Niekisch EA, Scharl G. *Solar Energy Mater.* 1980, 4, 101–112.
[13] Harish S, Sabarinathan M, Archana J, Navaneethan M, Ponnusamy S, Muthamizhchelvan C, Ikeda H, Hayakawa Y. *Appl. Surf. Sci.* 2017, 418, 171–178.
[14] Xu L, Zhou Y, Wu Z, Zheng G, He J, Zhou Y. *J. Phys. Chem. Solids* 2017, 106, 29–36.
[15] Adamu H, McCue AJ, Taylor RSF, Manyar HG, Anderson JA. *Appl. Catal. B Environ.* 2017, 217, 181–191.
[16] Wu S-C, Tan C-S, Huang MH. *Adv. Funct. Mater.* 2017, 27, 1604635–1604643.
[17] Lahmar H, Setifi F, Azizi A, Schmerber G, Dinia A. *J. Alloys Compd.* 2017, 718, 36–45.
[18] Geioushy RA, Khaled MM, Alhooshani K, Hakeem AS, Rinaldi A. *Electrochim. Acta* 2017, 245, 448–454.
[19] Hong W, Meng M, Liu Q, Gao D, Kang C, Huang S, Zhou Z, Chen C. *Res. Chem. Intermed.* 2016, 43, 2517–2528.
[20] Nishi Y, Miyata T, Minami T. *J. Vacuum Sci. Technol. A* 2012, 30, 4–6.
[21] Yu J, Chen Z, Wang Y, Ma Y, Feng Z, Lin H, Wu Y, Zhao L, He Y. *J. Mater. Sci.* 2018, 53, 7453–7465.
[22] Zheng Y, Chen C, Zhan Y, Lin X, Zheng Q, Wei K, Zhu J, Zhu Y. *Inorg. Chem.* 2007, 46, 6675–6682.
[23] Han L, Wang D, Lu Y, Jiang T, Liu B, Lin Y. *J. Phys. Chem. C* 2011, 115, 22939–22944.
[24] Chen W, Zhang W, Chen L, Zeng L, Wei M. *J. Alloys Compd.* 2017, 723, 172–178.
[25] Zhou X, Xie Y, Ma J, Mi H, Yang J, Cheng J, Hoang TKA. *J. Alloys Compd.* 2017, 721, 8–17.
[26] Lalitha K, Sadanandam G, Kumari VD, Subrahmanyam M, Sreedhar B, Hebalkar NY. *J. Phys. Chem. C* 2010, 114, 22181–22189.
[27] He Y, Wang Y, Zhang L, Teng B, Fan M. *Appl. Catal. B Environm.* 2015, 168, 1–8.
[28] He Y, Cai J, Li T, Wu Y, Lin H, Zhao L, Luo M. *Chem. Eng. J.* 2013, 215, 721–730.
[29] Ullah R, Dutta J. *J. Hazard. Mater.* 2008, 156, 194–200.
[30] Huang L, Peng F, Wang H, Yu H, Li Z. *Catal. Commun.* 2009, 10, 1839–1843.
[31] Yu J, Nong Q, Jiang X, Liu X, Wu Y, He Y. *Solar Energy* 2016, 139, 355–364.
[32] Li TB, Chen G, Zhou C, Shen ZY, Jin RC, Sun JX. *Dalton Trans.* 2011, 40, 6751–6758.
[33] Fu HB, Pan CS, Yao WQ, Zhu YF. *J. Phys. Chem. B* 2005, 109, 22432–22439.
[34] Su E-C, Huang B-S, Wey M-Y. *Acs Sustain. Chem. Eng.* 2017, 5, 2146–2153.
[35] Kathalingam A, Vikraman D, Kim H-S, Park HJ. *Opt. Mater.* 2017, 66, 122–130.